Heat transfer in tube assemblies under conditions of laminar axial, transverse and inclined flow

K. A. Antonopoulos*

This paper considers laminar flow heat transfer in tube assemblies. The main interest is focused on the virtually unexplored cases of heat transfer under conditions of fully-developed flow inclined to the axes of the tubes and of purely transverse developing flow. The limiting cases of purely axial or purely transverse fully-developed flow are also examined. In all cases, the thermal boundary condition on the tubes is constant heat flux. Governing differential equations are expressed in terms of curvilinear-orthogonal coordinates and solved using finite-differences. Results are compared with available theoretical and experimental data. The effect of the transverse component of the flow on the temperature distribution is found to remain very strong even in nearly-axial flows and therefore considerably higher heat transfer coefficients are exhibited by a nearly-axial flow than a purely axial one

Keywords: *heat transfer, laminar flow, tube assemblies, inclined flow*

Heat transfer aspects of a computational study of laminar flow heat transfer in tube assemblies are presented here. The hydrodynamic aspects were covered elsewhere[1,2].

Tube assemblies (Fig 1(a)) feature in many types of industrial equipment including heat exchangers, boilers, condensers and nuclear reactors. The simplest cases of heat transfer in tube assemblies occur under conditions of purely 'axial' fully-developed flow, for example in a nuclear reactor fuel assembly with heat extracted by a parallel flow of coolant, or under conditions of purely 'transverse' fully-developed flow, found in certain types of heat exchangers in which one stream is directed normal to the tube axes. These limiting cases are rare in practice. Thus, for example, there may be insufficient space for flow and heat transfer development; baffles may be introduced to change the flow direction to increase heat transfer, thus resulting in a flow inclined to the tube axes (Fig 1(a)). The latter cases are those of primary interest here.

Previous theoretical analyses of heat transfer in tube assemblies[1] have been confined to the limiting cases of the fully-developed purely axial and purely transverse flow. The studies of Sparrow *et al*[3] (laminar), Dwyer and Berry[4], Pfann[5] and Deissler and Taylor[6] (turbulent) are typical of the first case and those of Le Feuvre[7] and Massey[8] (laminar and turbulent) of the second. All of these studies are based on a numerical solution of the governing differential equations except for the solution of Sparrow *et al* which is analytical.

The limiting cases of heat transfer under conditions of fully-developed purely axial and purely transverse flow are examined here, although the main objective is to give an insight into the hitherto almost unexplored cases of heat transfer under conditions of fully-developed inclined flow and of developing purely transverse flow. The method of investigation is computation, ie the governing differential equations are expressed in terms of curvilinear-orthogonal coordinates and solved numerically using finite-differences. The calculations reported here concern laminar flow; current explorations of turbulent flow will be reported in a later publication.

Differential equations and coordinate system

The solution domain is of the irregular shape shown in the examples of Fig 1(b) (cross-sectional view) and in enlarged isometric view in Fig 1(c). To map this domain completely so that all boundaries are traced by coordinate surfaces, the coordinate frame $\xi-\eta-\zeta$ (Fig 1(c)) is employed; coordinates ξ and η on the cross-sectional plane are orthogonal-curvilinear while ζ is rectilinear and is aligned in the axial direction.

The transport equations governing steady three-dimensional viscous flow and heat transfer, in terms of the coordinates ξ, η and ζ, can be written in the following common form:

$$\frac{1}{l_\xi l_\eta}\frac{\partial}{\partial\xi}(\rho u l_\eta \Phi)+\frac{1}{l_\xi l_\eta}\frac{\partial}{\partial\eta}(\rho v l_\xi \Phi)+\frac{\partial}{\partial\zeta}(\rho w\Phi) - \frac{1}{l_\xi l_\eta}\frac{\partial}{\partial\xi}\left(\Gamma_\Phi \frac{l_\eta}{l_\xi}\frac{\partial\Phi}{\partial\xi}\right) - \frac{1}{l_\xi l_\eta}\frac{\partial}{\partial\eta}\left(\Gamma_\Phi \frac{l_\xi}{l_\eta}\frac{\partial\Phi}{\partial\eta}\right)-\frac{\partial}{\partial\zeta}\left(\Gamma_\Phi\frac{\partial\Phi}{\partial\zeta}\right)-S_\Phi=0 \quad (1)$$

where Φ is the dependent variable and may stand for the velocity components u, v, w, in the ξ, η, ζ directions respectively (Table 1) and for the temperature T(ie $\Phi=u$, v, w, T). S_Φ is the source of the property Φ: when Φ stands for any of the velocity components, S_Φ contains the

* National Technical University of Athens, Mechanical Engineering Department, Thermal Section, 42 Patission Street, Athens 106 82, Greece

Received 21 September 1984 and accepted for publication on 25 February 1985

 0142–727X/85/030193–12$3.00

appropriate pressure gradient term as well as terms arising from the coordinate curvature[1]. When Φ stands for the temperature T, S_Φ is taken to be zero. The term Γ_Φ in Eq (1) is the 'exchange coefficient' for property Φ: thus when Φ stands for the velocity components, Γ_Φ is the viscosity μ while when Φ stands for the temperature, Γ_Φ is the ratio k/c_p of the thermal conductivity to the specific heat of the fluid. Associated with the coordinates ξ and η are the spatially-varying metric coefficients l_ξ and l_η respectively, which link increments of curvilinear coordinate and physical distance. The continuity relationship closes the set of equations, ie:

$$\frac{1}{l_\xi l_\eta}\frac{\partial}{\partial\xi}(\rho u l_\eta)+\frac{1}{l_\xi l_\eta}\frac{\partial}{\partial\eta}(\rho v l_\xi)+\frac{\partial}{\partial\zeta}(\rho w)=0 \qquad (2)$$

Boundary conditions

The boundaries of the solution domain (Fig 1(c)) include symmetry planes, solid walls and inlet and outlet planes. On a symmetry plane the velocity normal to this symmetry plane is zero as are the normal gradients of temperature and of all other variables. On a tube wall the velocity components are set to zero and the temperature or heat flux is prescribed.

The boundary conditions at the inlet and outlet planes depend on the heat transfer case to be simulated. These boundary conditions and the manner of imposing them are discussed when the various heat transfer cases are examined.

Solution procedure

The solution procedure is based on the finite-difference formulation of Caretto *et al*[9] suitably modified[1,2] to incorporate the orthogonal-curvilinear coordinates. Accordingly only a brief outline of the solution procedure is given here.

A typical computational mesh employed for the

Notation

A_c	Cross-sectional area of a subchannel
a	Coefficient in finite-difference equations
c_p	Specific heat at constant pressure
D	Tube diameter
h	Local heat transfer coefficient, $h=\dot{q}''_w/(T_w-T_{ba})$
$\bar{h}$	Average heat transfer coefficient, $\bar{h}=\frac{1}{\pi(D/2)}\int_0^\pi h\frac{D}{2}\,d\varphi$
k	Thermal conductivity
l_ξ, l_η	Metric coefficients associated with the coordinates ξ and η respectively
$\dot{m}_a, \dot{m}_c$	Mass flow rate in the axial and transverse directions respectively
Nu	Local Nusselt number, $Nu=\frac{\dot{q}''_w D}{k(T_w-T_b)}$, where for purely axial flow $T_b=T_{ba}$, for purely transverse flow $T_b=T_{bI}$ for $0°\leqslant\varphi\leqslant 90°$ and $T_b=T_{b0}$ for $90°\leqslant\varphi\leqslant 180°$, and for inclined flow $T_b=T_{bI}$
$\overline{Nu}$	Average Nusselt number, $\overline{Nu}=\frac{1}{\pi(D/2)}\int_0^\pi Nu\frac{D}{2}\,d\varphi$
P	Distance between axes of parallel tubes (pitch)
p	Local pressure
Pr	Prandtl number, $Pr=\mu c_p/k$
P_w	Wetted perimeter
$\dot{Q}$	Total heat input to the solution domain per unit of time
$\dot{q}''_w$	Local wall heat flux
Re_a	Axial Reynolds number, $Re_a=\rho\bar{w}D/\mu$
Re_c	Transverse Reynolds number, $Re_c=\rho\bar{u}D/\mu$
Re	Renolds number of an inclined flow, $Re=\rho\bar{U}D/\mu$
$\overline{St}$	Average Stanton number, $\overline{St}=\frac{1}{\pi(D/2)}\int_0^\pi\frac{\dot{q}''_w}{\rho\bar{u}c_p(T_w-T_{bI})}\frac{D}{2}\,d\varphi$
S_Φ	Source term in the transport equations
T	Local fluid temperature
T_b	Bulk fluid temperature taken as T_{ba}, T_{bI}, or T_{b0} depending on the case
T_{ba}	Bulk fluid temperature in the cross-section plane, $T_{ba}=\frac{1}{A_c\bar{w}}\int_{A_c} wT\,dA_c$
T_{bI}	Bulk fluid temperature at the inlet of the cross-section $T_{bI}=\int_{in}\rho u c_p T\,d\eta\Big/\int_{in}\rho u c_p\,d\eta$
T_{b0}	Bulk fluid temperature at the outlet of the cross-section, $T_{b0}=\int_{out}\rho u c_p T\,d\eta\Big/\int_{out}\rho u c_p\,d\eta$
T_w	Local wall temperature
T_a^*	Dimensionless temperature, $T_a^*=k(T-T_{ba})/(\dot{q}''_w P_w)$
T_c^*	Dimensionless temperature, $T_c^*=k(T-T_{bI})/(\dot{q}''_w P_w)$
$\bar{U}$	Mean velocity in the direction of an inclined flow
$u,v,w,$	Velocity components in the ξ, η, ζ directions respectively
$\bar{u}$	Mean transverse velocity through the minimum cross-section
$\bar{w}$	Mean axial velocity
Γ_Φ	Exchange coefficient for property Φ
ζ	Rectilinear coordinate in the axial direction
ξ,η	Curvilinear-orthogonal coordinates on the cross-sectional plane
Θ	Angle of inclination of the bulk velocity to the tube axes, $\Theta=\arctan(\bar{u}/\bar{w})$
μ	Molecular viscosity
μ_b	Bulk fluid viscosity
μ_w	Viscosity near tube wall
ρ	Fluid density
Φ	General dependent variable which may stand for u, v, w, T
φ	Angular position of a point on tube surface measured from the rear of the tube

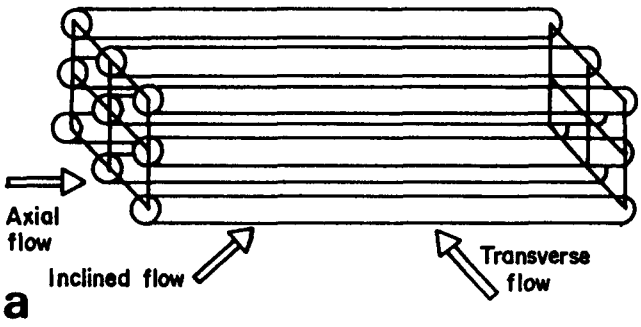

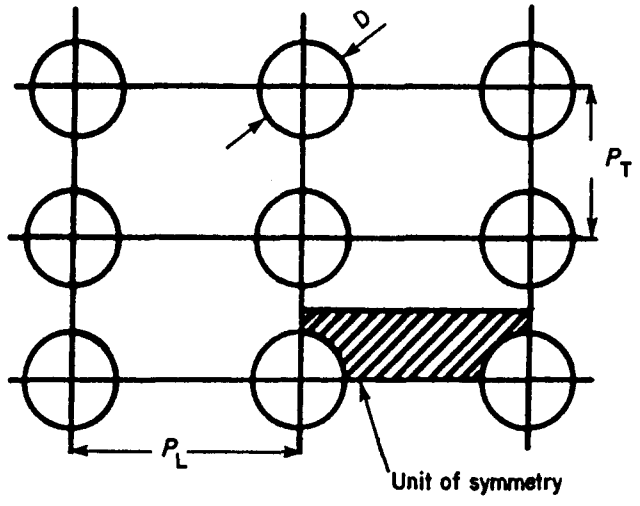

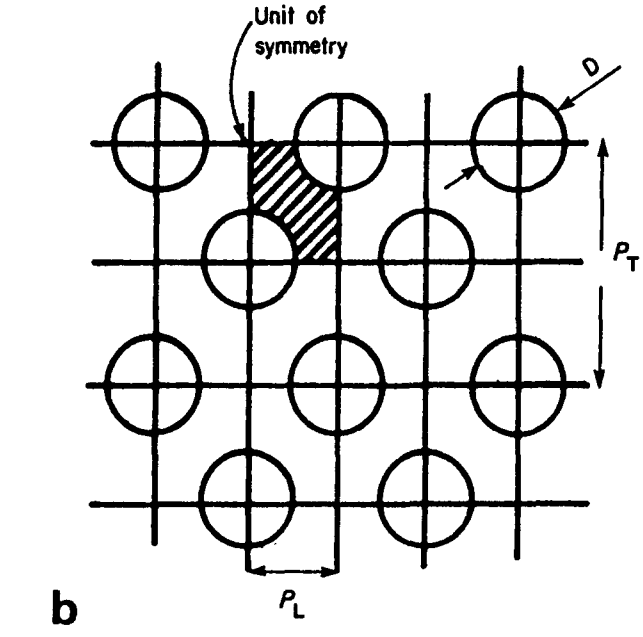

Fig 1 Flow in tube assemblies (a) axial, transverse and inclined flow, (b) in-line and staggered assemblies in cross-sectional view with indication of solution domain, (c) solution domain and coordinate system, (d) typical computational grid (cross-sectional view) with indication of control volume, and (e) solution domain with extra row of cells at the outlet used for the solution of fully-developed transverse or inclined flow

finite-difference solution of Eq (1) and (2) is shown in the example of Fig 1(d) (cross-sectional view). This is generated numerically to fit the irregular shape of the solution domain and the metric coefficient l_ξ, l_η and other required coordinate information are then deduced. The approach used is to solve the Laplacian differential transformation equations connecting the physical and curvilinear coordinates.

The differential momentum and energy equations (1) are cast into finite-difference form by integration over six-sided control volumes (Fig 1(d)) to yield equations of the form:

$$a_P\Phi_P = \sum_n a_n\Phi_n + S_{\Phi,P} \qquad (3)$$

$$n = E, W, N, S, D, U$$

where Φ stands for u, v, w and T, coefficients 'a' express the combined effects of convection and diffusion (approxi-

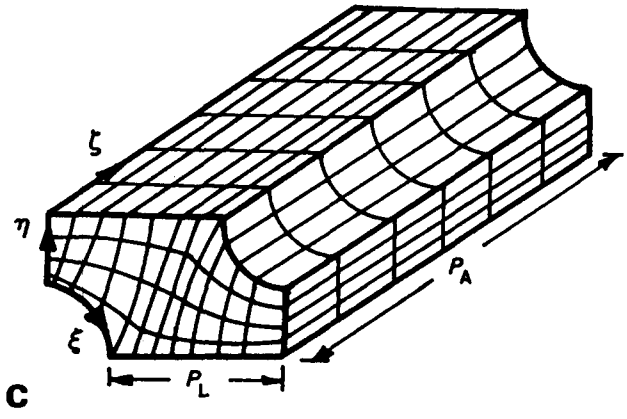

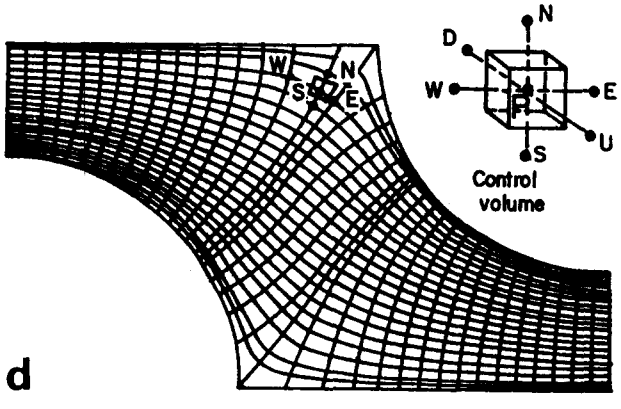

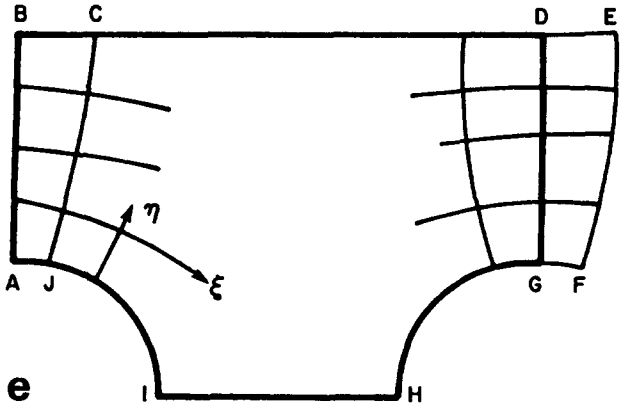

Table 1 Symbols in Eq (1)

Eq (1)	Variable Φ	Γ_Φ	S_Φ
ξ-momentum	u	μ	S_u
η-momentum	v	μ	S_v
ζ-momentum	w	μ	S_w
Energy	T	k/c_p	0

mated by a hybrid central/upwind difference operator); $S_{\Phi,P}$ contains central-difference approximations to the remaining terms; and the summation is over the neighbours E, W, N, S, D, U of the typical node P (Fig 1(d)) of each control volume. The continuity equation (2) is approximated by central differences and is used in conjunction with the momentum finite-difference equations to derive a pressure perturbation equation similar in form to Eq (3). The resulting equation set is solved by an iterative ADI (Alternating-Direction-Implicit) algorithm.

Heat transfer cases examined

Differential Eqs (1) and (2), which correspond to an arbitrary three-dimensional flow and heat transfer, are modified here to simulate heat transfer under conditions of:

(a) purely axial fully-developed flow (ie inclination angle $\Theta = \arctan(\bar{u}/\bar{w}) = 0°$)
(b) purely transverse fully-developed flow ($\Theta = 90°$)
(c) purely transverse developing flow ($\Theta = 90°$)
(d) fully-developed uniformly inclined flow ($0° < \Theta < 90°$).

The simplifications applied to Eqs (1) and (2) result in a considerable reduction in computer storage and time compared with the general case. Extracts are shown from a wide range of heat transfer prediction for these cases: corresponding results concerning hydrodynamics are given elsewhere[1,2].

Although the interest of the present work lies in the cases (c) and (d) above, the first two cases were included mainly to allow the accuracy of the method to be evaluated by comparison with existing theoretical and experimental data. This was particularly important because there is virtually no such information for the inclined and developing cases.

The fineness of the grids employed for the numerical solution of the governing equations in each case have been defined by performing grid dependence tests[1].

Heat transfer for purely axial fully-developed flow

Equations and boundary conditions

In this case (inclination angle $\Theta = 0°$) Eqs (1) and (2) are simplified as follows: first, the condition of full development of flow and heat transfer implies that all derivatives with respect to the axial coordinate ζ vanish, with the exception of terms $\partial p/\partial\zeta$ and $\partial(\rho wT)/\partial\zeta$. Also, transverse velocities u and v are set to zero. The problem is therefore described by the following equations:

Momentum equation in the ζ-direction:

$$\frac{1}{l_\xi l_\eta}\frac{\partial}{\partial\xi}\left(\mu\frac{l_\eta}{l_\xi}\frac{\partial w}{\partial\xi}\right)+\frac{1}{l_\xi l_\eta}\frac{\partial}{\partial\eta}\left(\mu\frac{l_\xi}{l_\eta}\frac{\partial w}{\partial\eta}\right)=\frac{\partial p}{\partial\zeta} \quad (4)$$

Energy equation:

$$\frac{\partial}{\partial\zeta}(\rho wT)-\frac{1}{l_\xi l_\eta}\frac{\partial}{\partial\xi}\left(\frac{k}{c_p}\frac{l_\eta}{l_\xi}\frac{\partial T}{\partial\xi}\right)-\frac{1}{l_\xi l_\eta}\frac{\partial}{\partial\eta}\left(\frac{k}{c_p}\frac{l_\xi}{l_\eta}\frac{\partial T}{\partial\eta}\right)=0 \quad (5)$$

The solution can therefore be confined to a single cross-sectional plane $\xi-\eta$ with the axial pressure gradient term $\partial p/\partial\zeta$ and the axial temperature gradient term $\partial(\rho wT)/\partial\zeta$ treated as follows: the term $\partial p/\partial\zeta$ is prescribed as an input or it is adjusted during the solution procedure so that the desired mass flow rate is obtained. Under the boundary condition of uniform wall heat flux $\dot{q}''_w$, the term $\partial(\rho wT)/\partial\zeta$ is explicitly known[10], ie:

$$\frac{\partial(\rho wT)}{\partial\zeta}=\rho w\left(\frac{\dot{q}''_w P_w}{\dot{m}_a c_p}\right) \quad (6)$$

where $\dot{m}_a$ is the mass flow rate and P_w the wetted perimeter. The above value of $\partial(\rho wT)/\partial\zeta$ is inserted as a source term during the solution of the energy Eq (5).

The boundary condition of uniform wall heat flux is used on the solid boundaries (ie tube surfaces AF and DE in Fig 2) of the solution domain while on all other boundaries (AB, BC, CD, EF in Fig 2) which are planes of symmetry, the normal gradients of temperature and velocity are set to zero.

Results

Computed contours of dimensionless temperature T_a^* (which by definition, is a function of geometry only) for a square arrangement of pitch-to-diameter ratio $P/D = 1.5$ are shown in Fig 2. The maximum T_a^* is obtained on the rod surface at locations coinciding with the narrowest passages and the minimum occurs at the centre of the cross-section, as expected.

It can be proven easily[1] that under the present conditions (ie purely axial fully-developed flow with uniform heat flux boundary condition) the mean Nusselt number $\overline{Nu}$ is constant, depending only on geometry. The $\overline{Nu}$ = constant relation has been verified by the present predictions and the results for the square and the equilateral triangular arrangements are shown in Fig 3 together with the Sparrow *et al*[3] analytical solution, which corresponds to the latter arrangement only. In addition to the excellent agreement between the two solutions, it can be seen that the equilateral triangular arrangement exhibits higher heat transfer rates than the square one because, for the same P/D, the former exhibits larger heated perimeter per flow area than the latter.

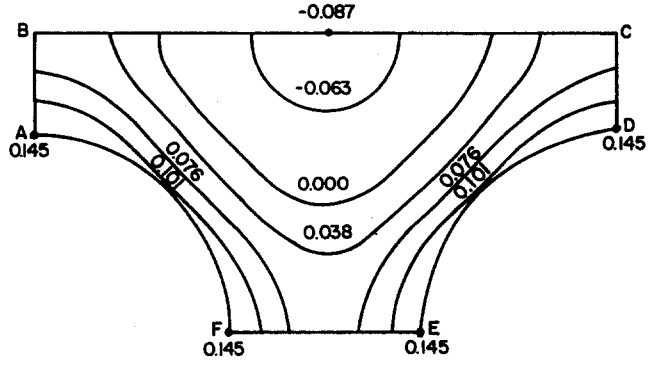

Fig 2 Predicted isotherms T_a^* for fully-developed purely axial flow through a square arrangement of P/D = 1.5

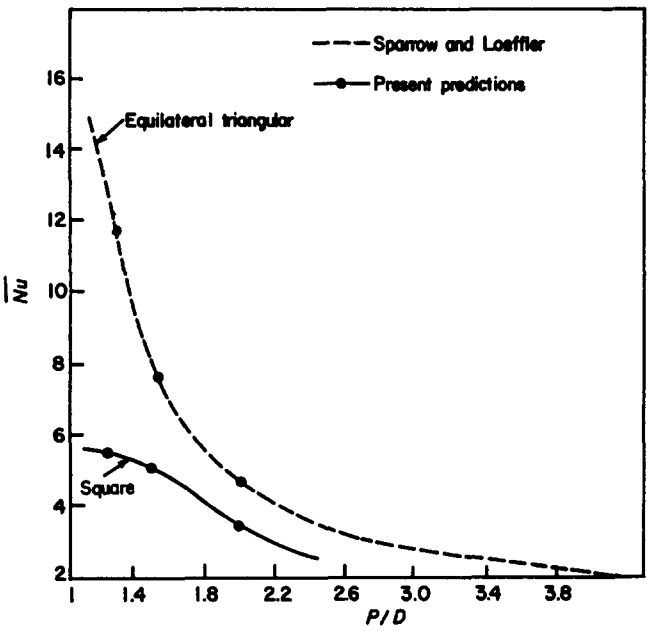

Fig 3 Predicted average Nusselt number $\overline{\mathrm{Nu}}$ *as a function of* P/D *for fully-developed purely axial flow*

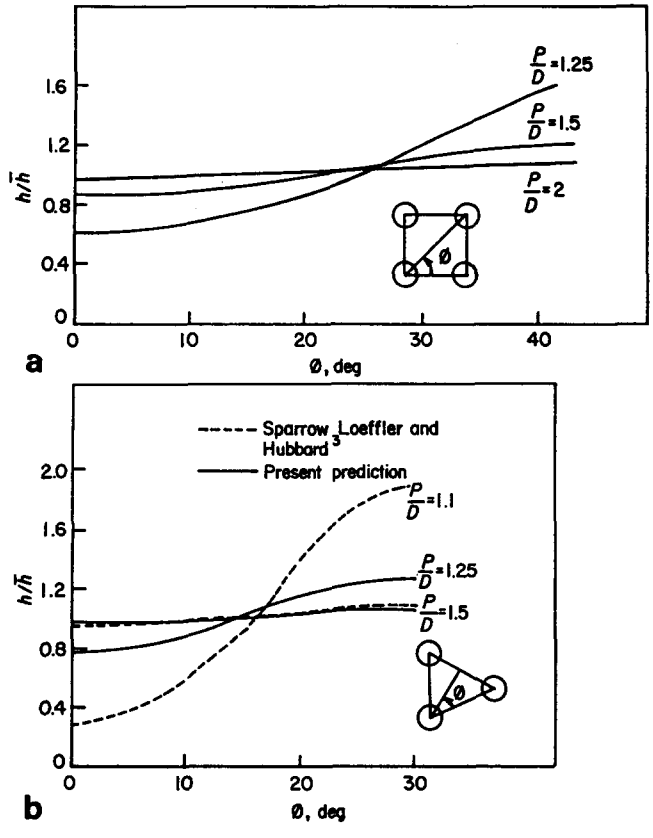

Fig. 4 Predicted local heat transfer coefficient distribution for fully-developed purely axial flow through (a) square arrangements of various P/D, *and (b) equilateral-triangular arrangements of various* P/D

The predicted variation of local heat transfer coefficient h around the rod surface is shown in Fig 4 for the square and the equilateral-triangular arrangements respectively. Significant circumferential variation exists for small P/D because the closer the spacing the more a rod is influenced by the presence of the surrounding rods; consequently, the velocity distribution is non-uniform and so is the heat transfer coefficient. For the same P/D a smaller circumferential variation is exhibited by the equilateral triangular array due to the larger number of neighbours surrounding each rod: flow and heat transfer are therefore more similar to those in an annular duct. It is noteworthy that, for both arrangements, the maximum heat transfer coefficient is observed at the location of the largest passage between the rods, where velocities are high, while the minimum occurs at the narrowest passage.

Fig 4(b) also shows the solution of Sparrow *et al*[3]. The agreement between the solutions, for $P/D=1.5$, is good.

Purely transverse fully-developed flow

Equations and boundary conditions

In this case (inclination angle $\Theta=90°$) the term in Eqs (1) and (2) relating to the axial coordinate ζ vanish and the axial velocity component w is set to zero. Therefore, the governing equations take the form:

Momentum equations in the ξ *and* η *directions* $(\Phi=u,v)$*:*

$$\frac{1}{l_\xi l_\eta}\frac{\partial}{\partial\xi}(\rho l_\eta u\Phi)+\frac{1}{l_\xi l_\eta}\frac{\partial}{\partial\eta}(\rho l_\xi v\Phi) -\frac{1}{l_\xi l_\eta}\frac{\partial}{\partial\xi}\left(\mu\frac{l_\eta}{l_\xi}\frac{\partial\Phi}{\partial\xi}\right)-\frac{1}{l_\xi l_\eta}\frac{\partial}{\partial\eta}\left(\mu\frac{l_\xi\partial\Phi}{l_\eta\partial\eta}\right)=S_\Phi \quad (7)$$

Energy equation:

$$\frac{1}{l_\xi l_\eta}\frac{\partial}{\partial\xi}(\rho l_\eta uT)+\frac{1}{l_\xi l_\eta}\frac{\partial}{\partial\eta}(\rho l_\xi vT) -\frac{1}{l_\xi l_\eta}\frac{\partial}{\partial\xi}\left(\frac{k}{c_p}\frac{l_\eta}{l_\xi}\frac{\partial T}{\partial\xi}\right)-\frac{1}{l_\xi l_\eta}\frac{\partial}{\partial\eta}\left(\frac{k}{c_p}\frac{l_\xi}{l_\eta}\frac{\partial T}{\partial\eta}\right)=0 \quad (8)$$

Continuity equation:

$$\frac{1}{l_\xi l_\eta}\frac{\partial}{\partial\xi}(\rho u l_\eta)+\frac{1}{l_\xi l_\eta}\frac{\partial}{\partial\eta}(\rho v l_\xi)=0 \quad (9)$$

Since no variations of flow conditions exist with axial direction ζ, the solution of these equations is confined to a single cross-sectional plane $\xi-\eta$. The condition of full development is used for the imposition of the boundary conditions at inlet BA and outlet DG of the solution domain (Fig 1(e)) as follows: the computational mesh is extended by one line EF and the temperature profile (as well as the profiles of the other variables) is transferred from line DG to line BA and from CJ to EF after each iteration during the solution. In this procedure, the increase in bulk fluid temperature DT_b is calculated as:

$$DT_b=\frac{\dot{Q}}{\dot{m}_c c_p} \quad (10)$$

where $\dot{Q}$ is the total heat input to the solution domain from the tubes per unit of time and $\dot{m}_c$ is the mass flow rate. DT_b is then subtracted from the temperature profile of line DG before this profile is inserted at line BA and similarly DT_b is added to that of line CJ before it is inserted at line EF.

An alternative procedure has also been devised[2] for imposing the repeating conditions at inlet and outlet. In this procedure, which leads to faster convergence, the

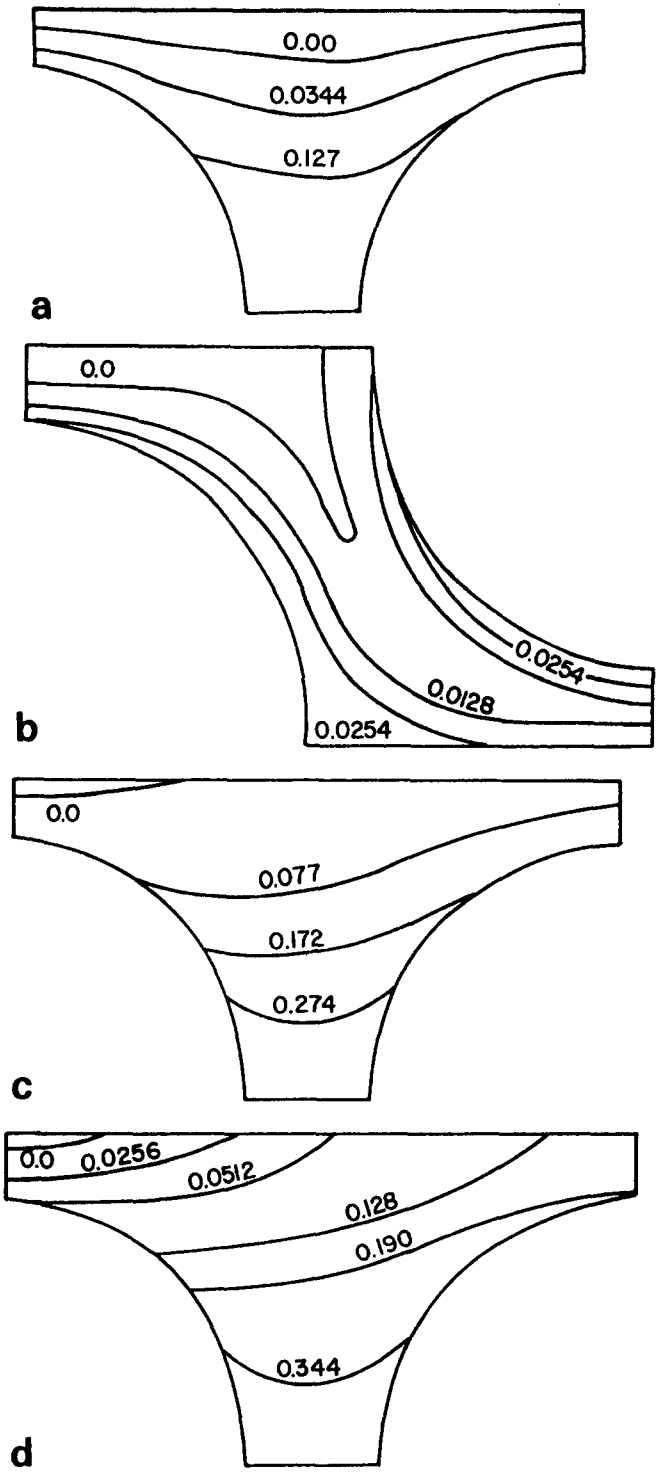

Fig 5 Predicted isotherms T_c^* *for fully-developed purely transverse flow through (a) an in-line square arrangement of* P/D = *1.25 for* Re_c = *50 and* Pr = *10, (b) an equilateral-triangular arrangement of* P/D = *1.25 for* Re_c = *50 and* Pr = *10, (c) an in-line square arrangement of* P/D = *1.25 for* Re_c = *10 and* Pr = *10, and (d) an in-line square arrangement of* P/D = *1.25 for* Re_c = *50 and* Pr = *1*

normal grid arrangement is used and the cyclic conditions are incorporated implicitly into the ADI algorithm.

The boundary condition of uniform heat flux $\dot{q}_w''$ is used on the solid boundaries (ie tube walls AJI and HGF, Fig 1(e)) of the solution domain while on the upper and lower boundaries BCDE and IH (Fig 1(e)) respectively, which are planes of symmetry, v-velocity is zero as are the normal gradients of temperature and u-velocity.

Results

Predicted contours of dimensionless temperature T_c^* for in-line and staggered tube arrangements are shown in Fig 5 for various values of Reynolds, Re_c, and Prandtl, Pr, numbers.

Comparison of Figs 5(a) and 5(b) reveals that for fixed values of Re_c and Pr, higher T_c^* are developed within the in-line subchannel (Fig 5(a)) than within the staggered one (Fig 5(b)). Heat is not, therefore, easily removed from the gap between the in-line tubes (recirculation zone), thus rendering the overall heat transfer poorer for the in line banks than for the staggered ones.

The influence of Re_c on the temperature distribution is shown by comparing Figs 5(a) and 5(c). A significant temperature rise along the flow centre line is observed at $Re_c = 10$ (Fig 5(c)) while the influence of flow field is strongly apparent at $Re_c = 50$ (Fig 5(a)), where the isotherms are biased towards the outlet of the cross-section. These characteristics show that, as expected, for low Re_c the temperature field is governed mainly by the effects of heat conduction, while for increasing Re_c the effect of convection becomes increasingly important.

Figs 5(a) and 5(d) illustrate the predicted influence of Pr on the temperature contours for an in-line arrangement at $Re_c = 50$. The isotherms for $Pr = 1$ (Fig 5(d)) indicate a significant temperature rise along the flow centre-line (ie strong influence of heat conduction) while for $Pr = 10$ (Fig 5(a)) the fluid in this region remains cool and the isotherms approximately follow the streamlines (ie the influence of convection is dominant).

The predicted distribution of the local Nusselt number Nu around the periphery of the rods for an in-line arrangement ($P/D = 1.5$, $Re_c = 100$, $Pr = 5$) is given in Fig 6(a), where comparison is made with Le Feuvre's[7] predictions for the same conditions. Agreement is good.

Fig 6(b) compares the prediced distribution of the local Nusselt number around the periphery of the tubes for an in-line arrangement ($P/D = 1.3$, $Re_c = 97$, $Pr = 528$) with Zhukauskas *et al*[11] measurements for the same conditions. Discrepancies of up to 15% are observed, which may be attributed to incomplete development of the flow and turbulence transition effects that may have been present in the experiments. The latter assumption is supported by the fact that the measured maximum Nu appears to be close to the reattachment point ($\varphi = 140°$). It is a turbulent flow characteristic to obtain maximum heat transfer at the reattachment point, where the near wall level of kinetic energy of turbulence attains a maximum value.

The predicted effect of Re_c on local Nu distribution around the tube periphery is shown in Fig 6(c), which corresponds to an in line arrangement of $P/D = 1.5$ for $Pr = 5$. The maximum Nu is obtained for both $Re_c = 10$ and $Re_c = 100$ on the top of the tubes ($\varphi = 90°$), where the highest velocity gradients occur, but the distribution for $Re_c = 10$ is more symmetrical than the one for $Re_c = 100$, where the convection effect is predominant.

The predicted distribution of local Nu for the in-line square tube banks of different spacing is shown in Fig 6(d) for $Re_c = 100$ and $Pr = 15$: for $P/D = 2$ the distribution of Nu is considerably more uniform than the corresponding one for $P/D = 1.5$, thus showing little effect of the surrounding rods. For the closely spaced tube bank, the

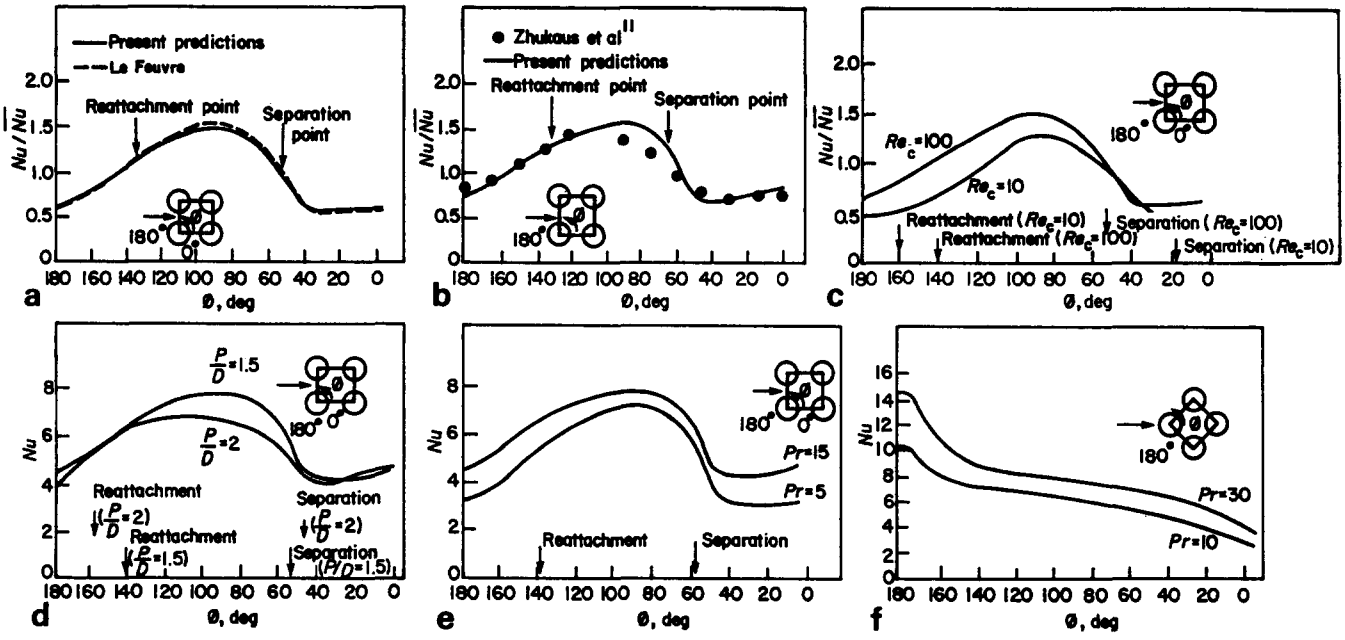

Fig 6 Predicted local Nusselt number distribution for fully-developed purely transverse flow through (a) an in-line square arrangement of P/D = *1.5 for* $Re_c = 100$ *and* Pr = *5, (b) an in-line square arrangement of* P/D = *1.3 for* $Re_c = 97$ *and* Pr = *528, (c) an in-line square arrangement of* P/D = *1.5 for various Reynolds numbers and* Pr = *5, (d) in-line square arrangements of* P/D = *1.5 and 2 for* $Re_c = 100$ *and* Pr = *15, (e) an in-line square arrangement of* P/D = *1.5 for* $Re_c = 100$ *and various Prandtl numbers, and (f) a staggered square arrangement of* P/D = *2.135 for* $Re_c = 10$ *and various Prandtl numbers*

maximum *Nu* occurs on the top of the tube while for the more widely spaced one it is relatively flat and extends towards the front of the tube, ie the region where the fluid is impinging. This region becomes important for widely spaced banks because it is affected less by the recirculation zone[1].

The predicted effect of *Pr* on the local *Nu* is shown in Fig 6(e) for an in-line square tube bank of $P/D = 1.5$ at $Re_c = 100$: higher *Nu* are obtained for higher *Pr* due to the increased temperature gradients near the tube surfaces, caused by the increased resistance to conduction. The influence of convection which causes the temperature gradients on the downstream tube to be greater than those on the upstream one, is also responsible for the asymmetry of *Nu* distribution about $\varphi = 90°$. For the higher *Pr*, *Nu* is more non-uniform, thus showing the stronger influence of convection. The predicted influence of *Pr* on the local *Nu* distribution for the staggered square arrangement is similar (Fig 6(f)).

Due to the geometrical dissimilarity between the in-line and staggered tube arrangements, their local heat transfer characteristics are dissimilar (Figs. 6(e) and (f)). The maximum *Nu* is generally expected to occur in the region of the highest velocity gradients or around the stagnation point where the fluid is impinging. For the in-line tube bank (Fig 6(e)) maximum *Nu* is at $\varphi = 90°$, ie in the region of the highest velocity gradients because the front of the tubes, where fluid should impinge, is covered by the recirculation zone[1]. For the staggered arrangement (Fig 6(f)), however, a flat maximum is obtained around the stagnation point ($\varphi = 180°$) since now recirculation appears only behind the tubes[1].

Fig 7 compares the predicted average Stanton numbers at various Re_c for both in-line square and staggered-square tube arrangements with the experimental data of Bergelin *et al*[12] and with Massey's

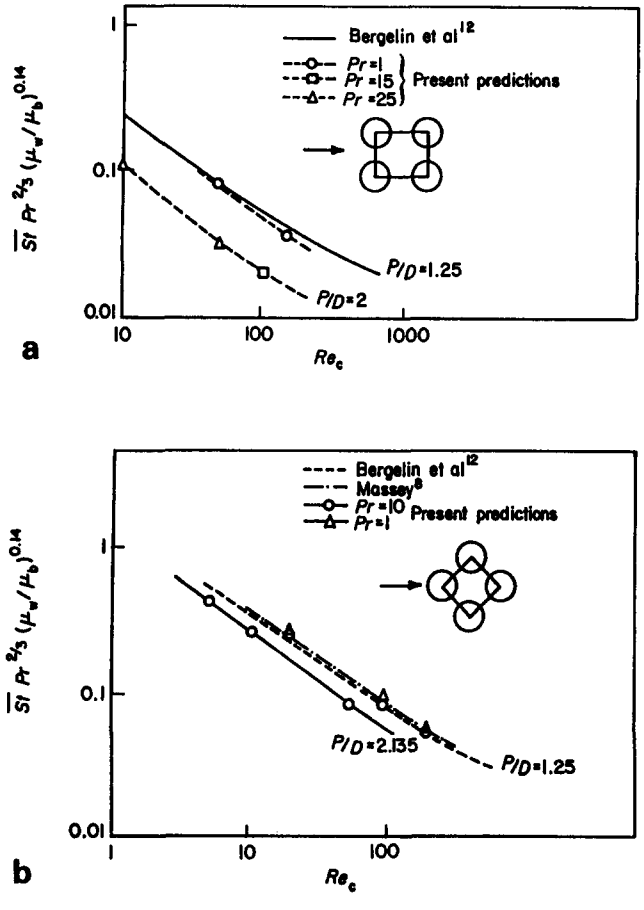

Fig 7 'Modified' average Stanton numbers for fully-developed purely transverse flow through (a) in-line square arrangements of various P/D *and (b) staggered square arrangements of various* P/D

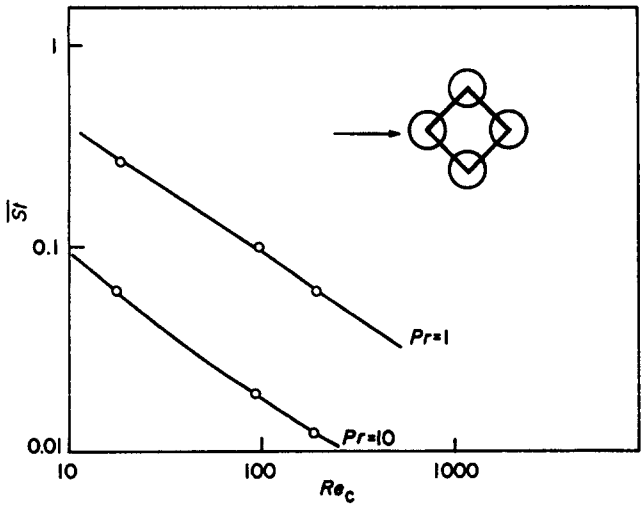

Fig 8 Predicted average Stanton number for fully-developed purely transverse flow through a staggered square arrangement of P/D = *1.25 for* Pr = *1 and 10*

numerical predictions[8]. Good agreement is obtained between the present predictions and the Bergelin *et al* data for the in-line arrangement (Fig 7(a)) provided $Re_c < 100$. For $Re_c > 100$ discrepancies are observed, probably due to the start of the transition to turbulent flow. For the staggered arrangement (Fig 7(b)) the present predictions lie between the experimental data and Massey's predictions, agreement with both being satisfactory. For both arrangements the small disagreement with Bergelin *et al* experiments may be due to the present calculations being made for uniform field properties (which vary during the experiments) on the basis that the experimental correlation (ie the use of $\overline{St}\ Pr^{2/3}(\mu_w/\mu_b)^{0.14}$) was proposed to allow for property variations: one can see in Fig 7(b) that for the staggered-square arrangement of $P/D = 1.25$, the present predictions for $Pr = 1$ are condensed to within 7% of those for $Pr = 10$.

The effect of geometry on the overall heat transfer is illustrated in Fig 7: closely-spaced banks, where a greater ratio of heating surface per flow area is available and steeper velocity gradients occur, exhibit superior heat transfer properties than widely-spaced ones. For constant P/D, staggered arrangements exhibit superior heat transfer properties.

The effect of Pr on the average heat transfer is illustrated in Fig 8, in the form of a plot of $\overline{St}$ against Re_c for various Pr. The curves are almost parallel, suggesting that the effect of Pr can be eliminated by using as ordinate the product $\overline{St}\ Pr^c$, where c is a constant, illustrated in Fig 7(b) where c = 2/3.

Purely transverse thermal developing flow

Equations and boundary conditions

In this case ($\Theta = 90°$) the problem is described by the same equations (Eqs (7)–(9)) which correspond to the fully-developed situation. The solution is again confined to a single cross-sectional plane $\xi - \eta$.

As the flow enters laterally through the outer periphery of the assembly with some arbitrary (but axially invariant) inlet distribution it is successively changed as it passes through successive rows of tubes; it is of interest to predict the heat transfer development. It would be expensive, however, to extend the solution domain to cover a large number of flow channels, so the practice followed is to solve the governing equations in one channel after another, with the inflow boundary conditions for the one considered being obtained from the predicted outflow of the preceding channel. To allow this, each solution domain is extended by one line EF (Fig 1(e)) to overlap slightly with the domain of the following channel, such that an interior grid line coincides with the inflow boundary of the downstream channel. After the solution for the first channel is obtained, the resulting profiles at that grid line are inserted at inflow boundaries in the calculation for the next channel. The outflow boundary conditions can only be estimated in this procedure: they are obtained by linear extrapolation of the variables from the interior, although other practices are possible.

The boundary conditions imposed on the tube walls and the upper and lower boundaries are the same as for fully-developed transverse flow.

Results

Calculations were performed for an in-line square arrangement of $P/D = 1.5$ at $Re_c = 50$ and 200 supplied with uniform velocity and temperature distributions at the inlet of the first row of tubes. The results are illustrated in Fig. 9, where both the local $\overline{St}$ (referred to the heat transfer within each individual subchannel) and the integrated value (referred to the overall heat transfer between the entry and the row of tubes in question) are plotted in terms of the number of rows. The local values show rapid heat transfer development, but also show that significantly higher $\overline{St}$ occur in the first two subchannels (the initial value is about 100% higher than the fully-developed one at $Re_c = 50$, and 150% higher at $Re_c = 200$) whose effects on the integrated values persist some considerable distance downstream.

No detailed data have been found against which these predictions may be tested, but two data points have been plotted in the above figure, corresponding to the integrated $\overline{St}$ measurements of Bergelin *et al*[12]: these were obtained in a ten-row assembly which, according to the present predictions, would have reflected small, but significant, entry effects in the measurements. The present predictions, however, still fall slightly below the data.

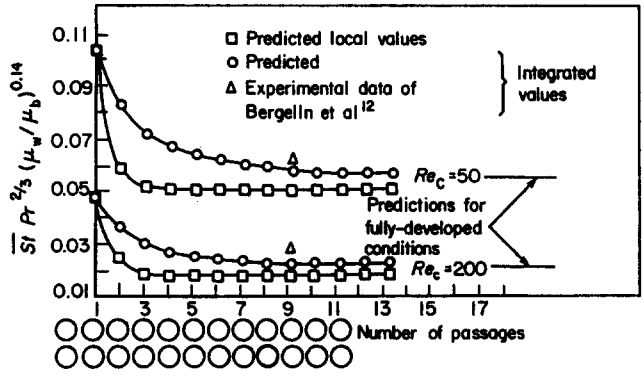

Fig 9 Predicted 'modified' average Stanton number for developing purely transverse flow as a function of number of passages through an in-line square arrangement of P/D = *1.5 at* Re_c = *50 and 200*

Uniformly inclined fully-developed flow

Equations and boundary conditions

In this case it is assumed that the bulk velocity vector makes everywhere the same angle with the tubes. The condition of full development of flow and heat transfer implies that all derivatives in Eqs (1) and (2) with respect to the axial coordinate ζ vanish, with the exception of the axial pressure gradient term $\partial p/\partial\zeta$ and the axial temperature gradient term $\partial(\rho wT)/\partial\zeta$. The momentum equations in the ξ, η, ζ directions therefore take the form of Eq (7) (for $\Phi = u, v, w$) and the continuity relationship takes the form of Eq (9). The energy equation becomes:

$$\frac{1}{l_\xi l_\eta}\frac{\partial}{\partial\xi}(\rho l_\eta uT)+\frac{1}{l_\xi l_\eta}\frac{\partial}{\partial\eta}(\rho l_\xi vT)+\frac{\partial}{\partial\zeta}(\rho wT)$$
$$-\frac{1}{l_\xi l_\eta}\frac{\partial}{\partial\xi}\left(\frac{k}{c_p}\frac{l_\eta}{l_\xi}\frac{\partial T}{\partial\xi}\right)-\frac{1}{l_\xi l_\eta}\frac{\partial}{\partial\eta}\left(\frac{k}{c_p}\frac{l_\xi}{l_\eta}\frac{\partial T}{\partial\eta}\right)=0 \quad (11)$$

Because of the simplifications performed, the solution can be confined to a single cross-sectional plane $\xi-\eta$ with the terms $\partial p/\partial\zeta$ (contained in the source term of w-momentum equation) and $\partial(\rho wT)/\partial\zeta$ treated as follows. The term $\partial p/\partial\zeta$ is prescribed as an input or it is adjusted during the solution procedure so that the desired axial mass flow rate may be obtained, as was the case with purely axial flow. The term $\partial(\rho wT)/\partial\zeta$, for the case of the uniform wall heat flux boundary conditions, can be easily calculated[1] as:

$$\frac{\partial(\rho wT)}{\partial\zeta}=\rho w\left(\frac{\dot{Q}\cos\Theta}{\dot{m}_c c_p P_L\sin\Theta+\dot{m}_a c_p P_A\cos\Theta}\right) \quad (12)$$

where P_L is the longitudinal pitch of the bank and P_A is the dimension of the solution domain in the axial direction (Fig. 1(c)). It is then inserted as a source term in the energy equation (11), as with the purely axial flow.

The condition of full development in the transverse direction is employed to impose the repeating conditions at boundaries BA and DG of the solution domain (Fig 1(e)) in the same manner as in the case of purely transverse fully-developed flow, with the exception that the increase in bulk fluid temperature DT_b is not, in this instance, calculated by Eq (10), but by:

$$DT_b=(T_b)_{DG}-(T_b)_{BA} \quad (13)$$

where $(T_b)_{DG}$ is the bulk temperature through line DG (Fig 1(e)) given by:

$$(T_b)_{DG}=\frac{\int_{DG}\rho uc_p T\,d\eta}{\int_{DG}\rho uc_p\,d\eta} \quad (14)$$

and $(T_b)_{BA}$ is the bulk temperature through line BA, given by an analogous equation.

The boundary condition of uniform wall heat flux is imposed on the solid boundaries (ie tube walls AJI and HGF, Fig 1(e)) of the solution domain while on the boundaries BCDE and IH, which are planes of symmetry, v-velocity is zero as are the normal gradients of temperature and of all other variables.

Results

Fig 10(a) compares predicted dimensionless temperature contours T_a^* for purely axial flow ($\Theta=0°$) and inclined flow ($\Theta=40.5°$) for an in-line square arrangement of $P/D=1.25$ for $Pr=10$. For $\Theta=0°$ the isotherms are symmetrical as expected but for $\Theta=40.5°$ they are all biased towards the outlet of the cross-section, thus showing the influence of the transverse component of the flow. Lower temperature gradients are observed for $\Theta=40.5°$ than for $\Theta=0°$ thus showing that higher heat transfer coefficients are expected for an inclined flow than for a purely axial one.

Fig 10(b) compares predicted dimensionless temperature contours T_c^* for purely transverse flow ($\Theta=90°$) and inclined flow ($\Theta=40.5°$) for the same tube arrangement and Prandtl number as above. The distortion of the isotherms between the tubes, in both the transverse and the inclined cases, is due to the recirculation zone of the transverse flow in this region[1]. Slightly less distortion is observed, however, for the inclined case due to the axial flow component which tends to offset the effect of transverse flow. Lower temperature gradients are observed in the inclined case. It is therefore expected that for the same Re_c, higher heat transfer coefficients will be exhibited by an inclined flow than a purely transverse one.

The effect of the transverse component of the flow on the temperature distribution within the cross-section remains very strong even in nearly-axial flows; Fig 10(c) compares the isotherm T_a^* for a nearly-axial flow

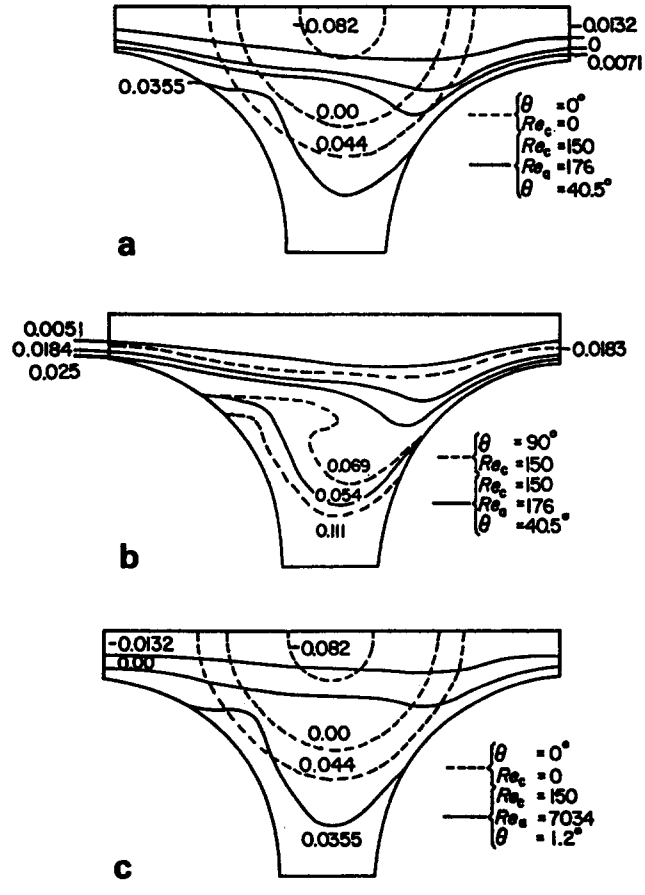

Fig 10 Predicted dimensionless temperature contours for fully-developed inclined flow through an in-line square arrangement of P/D = 1.25 for Pr = 10 (a) comparison with purely axial fully-developed flow, (b) comparison with purely transverse fully-developed flow, and (c) comparison with purely axial fully-developed flow

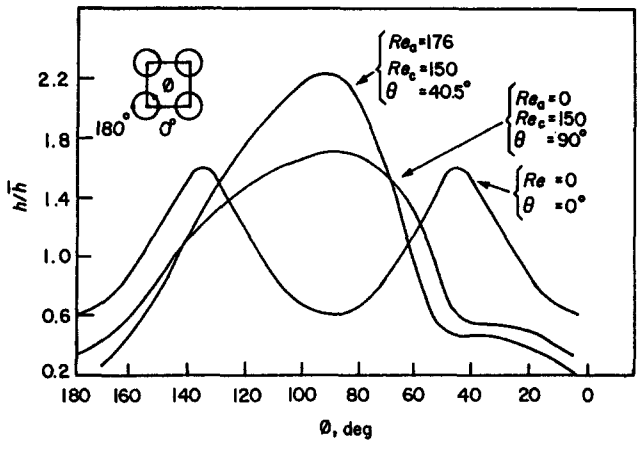

Fig. 11 Predicted distribution of local heat transfer coefficient for fully-developed inclined, axial and transverse flow through an in-line square arrangement of P/D = *1.25 at* Pr = *10*

($\Theta = 1.2°$) with those for a purely axial one ($\Theta = 0°$). The temperature gradients for $\Theta = 1.2°$ are lower than the ones for $\Theta = 0°$ and therefore better heat transfer is expected from a nearly-axial than from a purely axial flow.

The distorting influence of transverse flow on the distribution of the local heat-transfer coefficient h around the periphery of the tubes is shown in Fig 11, where $h/\bar{h}$ is plotted for $\Theta = 0°$, 40.5° and 90°. The h distribution for the inclined case ($\Theta = 40.5°$) is the most non-uniform but it is much more similar in shape to the distribution for purely transverse flow ($\Theta = 90°$) than to that for purely axial flow ($\Theta = 0°$).

Fig 12 shows the predicted average Nusselt number $\overline{Nu}$ as a function of the axial Reynolds number Re_a for various values of the transverse Reynolds number Re_c. Fig 12(a) is for in-line square arrangements of $P/D = 2$ at $Pr = 50$ and Fig 12(b) for $P/D = 1.25$ at $Pr = 10$; the inclination angles Θ are marked at various locations along the curves. The line corresponding to $Re_c = 0$ (ie $\Theta = 0°$, purely axial flow) is a straight line of zero slope, ie $\overline{Nu}$ is independent of Re_a, as mentioned earlier. For constant non-zero Re_c, however, the pattern of the curves differs:

(i) For Θ greater than about 85°, $\overline{Nu}$ is practically constant and equal to its corresponding purely-transverse flow value because the effect of the axial component of the inclined flow is negligible.

(ii) For intermediate values of Θ, ie $10° < \Theta < 85°$, $\overline{Nu}$ smoothly increases with Re_a because, due to the increasing axial component of the inclined flow, the thickness of the boundary layer on the tube surfaces decreases thus increasing heat transfer.

(iii) For the lower non-zero values of Θ (ie $\Theta < 10°$), $\overline{Nu}$ becomes practically constant for each constant value of Re_c. The explanation for this is that since the cross-flow velocities are now very small compared to the axial component, the $\overline{Nu}$ = constant behaviour of purely-axial flow is recovered but $\overline{Nu}$ is now higher than that for the latter case due to the effect of the transverse motions in distorting the axial velocity distribution. It should be emphasized that for a fully-developed inclined flow there is a strong and direct influence of the transverse flow field on the axial momentum distribution even if the former is very small compared to the axial component of the flow[1].

(iv) For very small values of Θ (ie $\Theta \to 0°$), $\overline{Nu}$ tends to its purely-axial flow value (but this does not appear in Fig 12).

A practically-important conclusion stemming from (iii) is that for highly-axial flows ($0° < \Theta < 10°$) $\overline{Nu}$ is a function of Re_c only. This function is shown in Fig 13 for an in-line square arrangement of $P/D = 2$ for $Pr = 50$.

The predicted effect of inclination on the overall heat-transfer behaviour is shown in a more compact form in the correlation of Fig 14(b), where $\overline{Nu}$ is plotted versus the Reynolds number Re of the inclined flow for various inclination angles Θ. For Θ = constant, $\overline{Nu}$ increases with Re as is the case with purely transverse flow. For Re = constant, $\overline{Nu}$ increases with Θ (the maximum $\overline{Nu}$ being obtained for purely transverse flow) in a non-uniform way: a rapid increase is observed for small values of Θ (ie $\Theta < 45°$) while for higher Θ the rate of increase falls. Comparison of Figs 14(a) with 14(b) reveals that these trends are in agreement with those predicted by the Dwyer correlation[13]:

$$\overline{Nu} = f\left(\frac{\sin\Theta + \sin^2\Theta}{1+\sin^2\Theta}\right)^{1/2}(4.6 + 0.193Pe^{0.614}) \qquad (15)$$

where f is a function of the geometrical characteristics of the tube bank and Pe is the Peclet number. The value of function f used in Fig 14(a) was found by tuning the correlation to fit the present predictions for purely transverse flow at $Re_c = 50$. However this correlation does not hold in the limiting case of purely axial flow, for which it

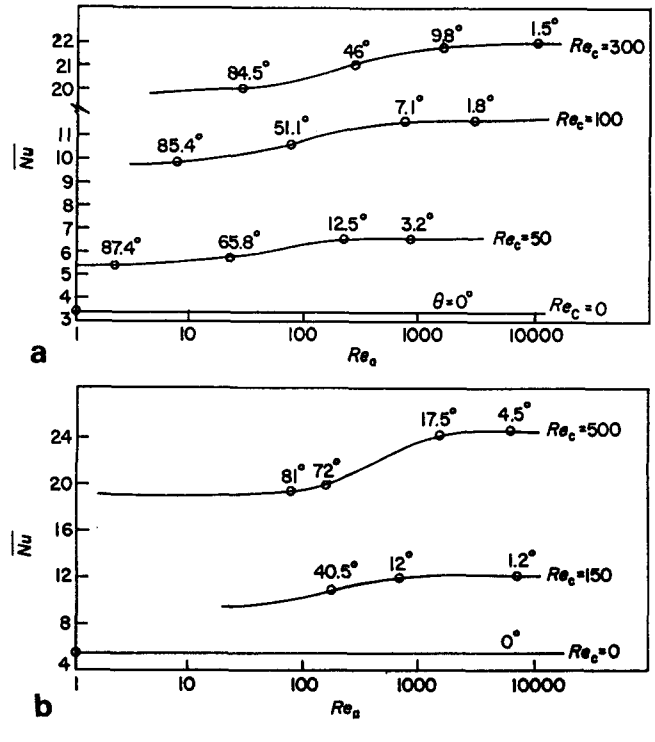

Fig 12 Predicted average Nusselt number as a function of the axial Reynolds number Re_a *for various transverse Reynolds numbers* Re_c, *for fully-developed inclined flow through an in-line square arrangement (a) of* P/D = *2 at* Pr = *50 and (b) of* P/D = *1.25 at* Pr = *10*

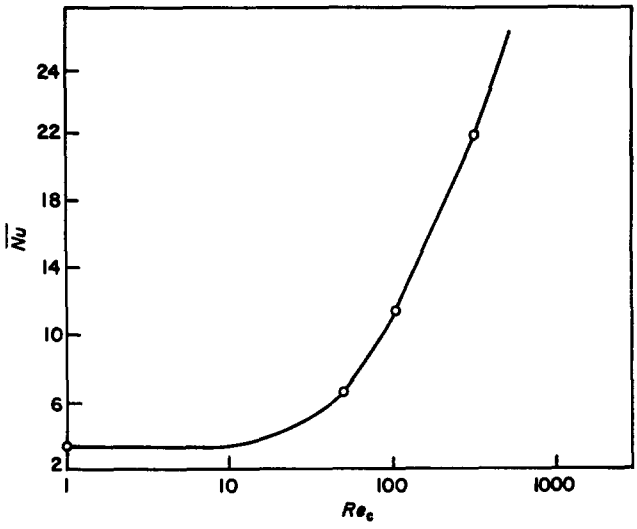

Fig 13 Predicted average Nusselt number as a function of the transverse Reynolds number Re_c *for fully-developed inclined flow with inclination angle* $0° < \Theta < 10°$ *through an in-line square arrangement of* P/D = 2 *at* Pr = 50

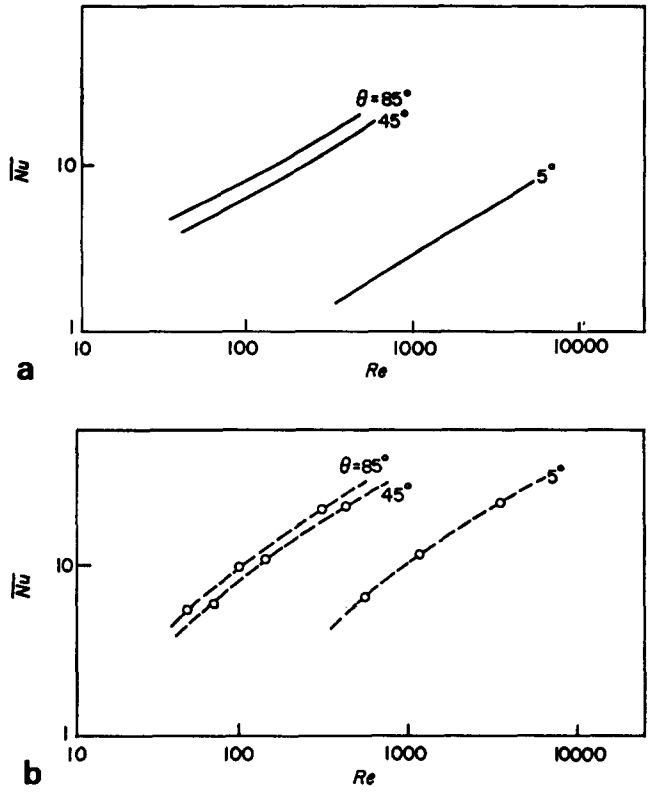

Fig 14 Average Nusselt number as a function of the Reynolds number Re *for fully-developed inclined flow through an in-line square arrangement of* P/D = 2 *for* Pr = 50 *(a) Dwyer correlation*[13] *and (b) present predictions*

underestimates $\overline{Nu}$ (ie it gives $\overline{Nu} = 0$ for $\Theta = 0°$). This is, probably, the reason why Eq (15) gives lower values of $\overline{Nu}$ at small Θ than the present predictions (Fig 14). For higher values of Θ, however, reasonable quantitative agreement is observed.

Conclusion

This prediction method has been successfully tested against experimental and theoretical data, mainly for heat transfer under conditions of fully-developed axial and transverse flow, as there was hardly any such information about the developing and inclined flow cases. It is concluded from the overall performance of the method that it allows calculations of heat transfer in tube banks to be made for a wider range of circumstances than has been possible to date.

It is believed that the results presented provide an insight into the hitherto almost unexplored situations of heat transfer under conditions of developing transverse and fully-developed inclined flow. The main findings include:

In the case of developing purely transverse flow, heat transfer develops rapidly for both low and high (laminar) Reynolds numbers, but also considerably higher Stanton numbers occur in the first two subchannels whose effect on the overall heat transfer persist a considerable distance down-stream.

Inclined flows exhibit superior heat transfer behaviour than a purely axial or a purely transverse flow with the same Reynolds and Prandtl numbers. The effect of the transverse component of the inclined flow is very strong even for highly-axial flows, thus rendering the distribution of the temperature and of the local heat transfer coefficient much more similar in shape to that of a purely transverse flow than to that of a purely axial one.

Although for a purely axial flow the average Nusselt number $\overline{Nu}$ is constant, for an inclined flow with fixed transverse Reynolds number Re_c, $\overline{Nu}$ is practically constant for the higher values of inclination angle Θ. $\overline{Nu}$ then increases with decreasing Θ and becomes again almost constant for the lower values of Θ (but not for Θ less than 0.2°, where $\overline{Nu}$ attains its purely axial flow value), ie the $\overline{Nu}$ = constant behaviour of purely axial flow is recovered but $\overline{Nu}$ is now higher than that for the latter case thus showing the strong influence of the transverse flow component even for highly axial flows.

At a fixed Reynolds number *Re* of the inclined flow, $\overline{Nu}$ increases with increasing Θ (in a decreasing rate as Θ tends to 90°), the maximum value being obtained for a purely transverse flow ($\Theta = 90°$) and the minimum for a purely axial one ($\Theta = 0°$). At a fixed Θ, $\overline{Nu}$ increases with *Re*.

Acknowledgements

The author gratefully acknowledges the assistance of Dr A. D. Gosman of Imperial College, London, UK.

References

1 **Antonopoulos K. A.** Prediction of flow and heat transfer in rod bundles, *PhD Thesis, Imperial College of Science and Technology, London University, 1979*

2 **Antonopoulos K. A., Gosman A. D. and Issa R. I.** Flow and heat transfer in tube assemblies, *Proc. 1st Int. Conf. on Numerical Methods in Laminar and Turbulent Flow, University College, Swansea, UK, Pentech Press, London, 1978*

3 **Sparrow E. M., Loeffler A. L. and Hubbard H. A.** Heat transfer to longitudinal laminar flow between cylinders, *J. of Heat Trans., Trans. ASME, 1961, 415–422*

4 **Dwyer O. E. and Berry H. C.** Heat transfer to liquid metals flowing turbulently and longitudinally through closely spaced rod bundles, part I, *Nuclear Eng. and Design, 1972,* **23**, *273–294*

5 **Pfann J.** Turbulent heat transfer to longitudinal flow through a triangular array of circular rods, *Nuclear Eng. and Design, 1975,* **34**, *203–219*

6 **Deissler R. G. and Taylor M. F.** Analysis of axial turbulent flow and heat transfer through banks of rods or tubes, *TID-7529, Reactor heat transfer Conference, New York, 1957, pt. 1, book 1, 416–461*

7 **Le Feuvre R. F.** Laminar and turbulent forced convection processes through in-line tube banks, *PhD Thesis, Imperial College of Science and Technology, London University, 1973*

8 **Massey T. H.** The prediction of flow and heat transfer in banks of tubes in cross-flow, *PhD Thesis, Central Electricity Research Laboratories, Leatherhead, Surrey, UK, 1976*

9 **Caretto L. S., Gosman A. D., Patankar S. V. and Spalding D. B.** Two calculation procedures for steady, three-dimensional flows with recirculation, *Proc. 3rd Int. Conf. on Numerical Methods in Fluid Mechanics, Springer Verlag, 1972, Vol 2, 60–68*

10 **Kays W. M.** Convective heat and mass transfer, *Tata MacGraw-Hill, New Delhi, 1975*

11 **Zhukauskas A., Makariaichius V. and Shanchiauskas A.** Heat transfer in banks of tubes in cross-flow of fluid, *Mintis, Vilnius, 1968*

12 **Bergelin O. P., Brown G. A. and Doberstein S. C.** Heat transfer and fluid friction during flow across banks of tubes, part IV, *Trans ASME, 1952,* **74**, *953–960*

13 **Dwyer O. E.** Liquid metal heat transfer, *BNL11936R, 1969*

CALENDAR

Direct and Large Eddy Simulation of Turbulent Flows (Euromech, colloquium)	30 September–1 October 1985 Munich, FRG	Professor R. Friedrich, Lehrstuhl für Stromungsmechanik, Technische University München, Acisstrasse 21, 8000 München 2, FRG
Measurement Techniques in Low-speed Turbulent Flows (Euromech. colloquium)	7–9 October 1985 Marknesse, The Netherlands	Dr B. van den Berg, National Aerospace Laboratory NLR, Voorsterweg 31, 8316 PR Marknesse, The Netherlands
Industrial Heat Exchanger Technology Symposium	6–8 November 1985 Pittsburgh, PA, USA	Conferences and Expositions, American Society for Metals, Metals Park, OH 44073, USA
ASME Winter Annual Meeting	17–21 November 1985 Miami, FL, USA	ASME, 345 East 47th Street, New York, NY 10017, USA
Fluid Transients in Fluid Structure Interaction – 2nd Symposium	17–21 November 1985 Miami, FL, USA	ASME, 345 East 47th Street, New York, NY 10017, USA
Fundamental Aspects of Gas Liquid Flows	17–21 November 1985 Miami, FL, USA	Professor E. E. Michaelides, Mechanical and Aerospace Engineering, University of Delaware, Newark, DE 19716, USA
Numerical Methods for Multiphase Flow (course)	18–22 November 1985 Ispra, Italy	Secretariat 'Ispra-Courses', Centro Commune di Ricerca, I-21020 Ispra (Varese), Italy
AIAA Joint Fluid Dynamics and Heat Transfer Conference	12–14 May 1986 Atlanta, GA, USA	American Institute of Aeronautics and Astronautics, 1290 Avenue of the America, New York, NY 10019, USA
Water for Energy	14–16 May 1986 Brighton, UK	BHRA Fluid Engineering Centre, Cranfield, Bedford MK43 0AJ, UK
31st International Gas Turbine Conference and Exhibit	8–12 June 1986 Dusseldorf, FRG	ASME, 345 E. 47th Street, New York, NY 10017, USA
Flow Measurement in the Mid-80s	9–12 June 1986 Glasgow, UK	Conference Section, National Engineering Laboratory, East Kilbride, Glasgow G75 0QU, UK
6th International Symposium: Finite Element Methods in Flow Problems	16–20 June 1986 Antibes, France	INRIA, Service des Relations Extérieures Rocquencourt, BP 105, 78153 Le Chesnay Cedex, France
8th International Heat Transfer Conference	17–22 August 1986 San Francisco, CA, USA	Chang-Lin Tien, Department of Mechanical Engineering, University of California, Berkeley, CA 94720, USA
7th International Fluid Power Symposium	16–18 September 1986 Bath, UK	BHRA, The Fluid Engineering Centre, Cranfield, Bedford MK43 OAL, UK
5th International Conference on Pressure Surges	22–24 September 1986 Hannover, FRG	BHRA Fluid Engineering Centre, Cranfield, Bedford MK43 0AJ, UK
ASME Winter Annual Meeting: International Symposium on Pressure and Temperature Measurement	30 November–5 December 1986 San Francisco, CA, USA	Dr J. H. Kim, Electric Power Research Institute, 3412 Hillview Avenue, PO Box 10412, Palo Alto, CA 94303, USA
Australian Fluid Mechanics Conference	8–12 December 1986 Auckland, New Zealand	AFMC Conference Committee, c/o Dr P. S. Jackson, Dept of Mechanical Engineering, Auckland University, Private Bag, Auckland, New Zealand